

Contents lists available at ScienceDirect

Cement and Concrete Composites

journal homepage: http://www.elsevier.com/locate/cemconcomp





Estimating reaction kinetics of cementitious pastes containing fly ash

Deborah Glosser^a, Prannoy Suraneni^b, O. Burkan Isgor^{a,*}, W. Jason Weiss^a

- ^a Civil and Construction Engineering, Oregon State University, Corvallis, OR, 97331, USA
- ^b Civil, Architectural and Environmental Engineering, University of Miami, Coral Gables, FL, 33146, USA

ARTICLE INFO

Keywords: Thermodynamic modeling Kinetic modeling Reactivity Fly ash Supplementary cementitious materials

ABSTRACT

This paper proposes an approach to estimate reaction kinetics for major fly ash glassy oxides in cementitious mixtures. The approach is compared to experimental results from multiple independent datasets. The kinetic model is based on the rate limiting step for various oxides and phases using the general form of a widely used model for ordinary portland cement (OPC)-based systems. The empirical parameters in the model were fit from dissolution studies for glass oxides in two fly ashes from literature using a nonlinear optimization algorithm. The outputs of the model provide the inputs needed to introduce reaction kinetics into thermodynamic simulations at non-equilibrium conditions. The model is used to determine the amount of each phase that can react by estimating the dissolved mass of each major cement phase and fly ash glass oxide at different ages. This approach enables accurate modeling predictions of solid hydration products (such as calcium hydroxide and ettringite), pore solution pH, and pore solution chemistry at any age for any OPC/fly ash system. Results from the model and thermodynamic calculations are compared to a modeling approach without kinetic constraints on the fly ash, assuming 100% reactivity. The prediction of reaction products made assuming 100% fly ash reactivity significantly differs from experimental values when a fly ash kinetic model is not used. Predictions are greatly improved when the model is used. The model can be used as a framework for future modeling efforts, and the empirical parameters be updated as additional dissolution studies and thermodynamic data become available.

1. Introduction

This paper describes a framework for accurate, non-equilibrium thermodynamic modeling of any OPC/fly ash mixture, based only on a priori knowledge of the ordinary portland cement (OPC) and supplementary cementitious material (SCM) chemical compositions. Thermodynamic modeling is a powerful tool to predict equilibrium reaction products and pore solution chemistry in cementitious systems [1-3]. One limitation of thermodynamic modeling is that it considers equilibrium conditions. However, cementitious systems are inherently non-equilibrium as they react [4]. Therefore, a kinetic framework to estimate dissolution rates of the cementitious phases at different ages is needed in order to perform thermodynamic modeling [5]. The Parrot-Killoh model (PK model) is an established method to describe the proportion of the four clinker phases in OPC that are available to react (i. e., dissolved into the pore solution at a given age) [1,6-8]. Given any combination of initial OPC chemical composition, the PK model computes the non-equilibrium inputs that describe the masses of each clinker phase at different ages used in thermodynamic simulations. While more complex atomistic [9-11], molecular dynamics [12,13], and microstructural simulation models [14,15] exist to describe the hydration processes and products in cementitious systems, these models are not necessarily designed to provide the outputs needed for thermodynamic simulation of cementitious mixtures [16]. Although recent work in modeling the pozzolanic reaction of fly ash has incorporated information on the dissolution of fly ash glasses [17], such models also do not provide the necessary data needed for thermodynamic simulations. Such outputs are important for the prediction of factors that control the durability of the mixtures because thermodynamic calculations allow for simulation of parameters such as strength development [18], porosity [8], and formation factor [19]. The model demonstrated in this paper, is designed explicitly as a framework to estimate the reaction kinetics in OPC/fly ash systems, so that thermodynamic modeling can be used to predict reaction products in any mixture, based only on a priori information on the system chemical composition.

The PK model fills an important need in cement science, and has been used to incorporate reaction kinetics into thermodynamic modeling as a function of time [1,2,20-22]. While the PK model is powerful, most

E-mail address: burkan.isgor@oregonstate.edu (O.B. Isgor).

https://doi.org/10.1016/j.cemconcomp.2020.103655

^{*} Corresponding author.

modern binders, contain SCM [23] such as fly ash, slag, or silica fume. In its current form, the PK model is limited to only the four major phases in OPC. An extension of the PK model is needed to provide the kinetic inputs required for thermodynamic modeling in systems that contain SCM. Previous work with thermodynamic modeling in OPC/SCM systems either used the PK model for the OPC phases and 1) made simplifying assumptions on the reactivity of the SCM phases, such as assuming constant reactivity [2,24,25]; or 2) fit a rate equation to the specific set of experimental data, that only described the particular system being modeled [3,26]. The limitation of the first option is that kinetics are not actually considered for the SCM, and the limitation of the second option is that experiments are necessary, and do not allow for simulation of other experimental conditions and compositions of SCM. Prior work has extended the PK model principles to OPC/amorphous silica mixtures [27], and here, this model framework (the modified Parrot-Killoh or MPK model) is applied to OPC/fly ash mixtures.

Fly ash, which is a byproduct of coal combustion [28] is a commonly used SCM that can show both hydraulic and pozzolanic reactions in OPC-based systems [29]. Thermodynamic modeling can be used to predict reaction products for any OPC/fly ash mixture, based only on the chemical compositions and environmental conditions only if the reaction kinetics of the fly ash dissolution can be accounted for. A kinetic model like the PK model is necessary for fly ash in order to achieve this objective. The MPK model, like the PK model, is based on empirical dissolution kinetics [30,31], as well as on the current scientific understanding of fly ash composition and structure [32–34].

Recent advances in scientific understanding of dissolution and reaction kinetics of fly ash show that typically the glassy (amorphous) components in fly ash are reactive in cementitious systems [17,32,35, 36]. It has been hypothesized that the intrinsic reactivity of fly ash can be described by the glass:crystalline ratio of the fly ash [17]. While the bulk composition is not irrelevant to the formation of reaction products, there is generally little correlation between the bulk composition of a fly ash and its glassy phase composition [31,37-39]. This paper, therefore, focuses on the role of glass in fly ash on reaction rates. Because experimental measurement of glass dissolution of individual fly ashes is at present complicated and limited [31], the model presented in this paper (based on dissolution studies of glass phases in two fly ashes [30]) is intended to serve as a framework for future modeling efforts. This framework can be modified as more calibration data becomes available, or as new model forms are developed. However, even at this early stage, this work demonstrates that even with provisional model coefficients, the MPK model produces relatively realistic estimations of fly ash glass dissolution kinetics, and accurate thermodynamic models for the solid and liquid reaction products in OPC/fly ash mixtures.

2. The MPK model

The MPK model is extended from describing OPC/amorphous silica systems [27] to include seven components: C_3A , C_2S , C_3S , C_4AF , amorphous SiO_2 , amorphous CaO, and amorphous Al_2O_3 . The later three oxides form the major reactive phases in most fly ashes [25].

The PK model calculates the dissolution rates of the four clinker phases at different ages, based on empirically determined dissolution coefficients. These coefficients have been shown to apply to the majority of cements [22], and therefore the modeling approach is applicable to most OPC systems. In the MPK model, the dissolution rate at time t is used to calculate the mass of each dissolved cement phase and fly ash oxide, or average system degree of hydration at a given age. The calculated dissolution rate is based on the slowest of the following processes: 1. nucleation/precipitation; 2. diffusion; and 3. reduction in transport of dissolved species, at a given time. That rate controlling step is then used in conjunction with a form of the Avrami equation [1] to determine the overall time-and temperature dependent dissolution of each phase. While it may be argued that the fundamental details of these processes may be improved, the ability to use the equations to describe

kinetics does not exist and is currently the most direct way to bring these data into thermodynamic calculations.

The MPK model contains a term DoR_{ph}^* , to describe the maximum degree of reactivity of each component. This term refers to the maximum mass % of each component that is capable of dissolving into solution (and participating in chemical kinetics) based on whether it is crystalline or amorphous (glassy). Prior work has demonstrated that typical crystalline phases found in fly ash are not capable of dissolving into solution in cementitious systems at room temperature [34,40–43]. The alkaline pH of the pore solution – combined with structural characteristics of the crystals – preclude their dissolution. While different glass structures also show variation in dissolution rates in fly ash (due in large part to polymerization and depolymerization of glass structures by network modifying cations in order to maintain charge balance) [31,41], all amorphous phases in fly ash are believed to be capable of dissolution. For the clinker phases and for silica fume, DoR_{ph}^* can be assumed to be

The MPK model calculates the time dependent dissolution rates and degrees of reaction, $\alpha_{ph}(t)$, of each of the seven phases and oxides in the OPC and fly ash (C $_3$ S, C $_2$ S, C $_3$ A, C $_4$ AF, amorphous SiO $_2$, amorphous Al $_2$ O $_3$, and amorphous CaO). The term "degree of reaction" as used here includes the hydraulic reactions of the clinker phases and the pozzolanic and hydraulic reactions of the fly ash glass oxides. The term is used in order to distinguish the time dependent reactions from the overall maximum degree of reactivity (DoR $_ph^*$) of the SCM.

The form and parameters of the MPK model are shown in Equations (1) and (2).

$$\alpha_{ph}(t) = \int_0^t DoR_{ph}^* \left(min \left\{ \frac{A_{ph}}{A_0} r_{ph,1}, r_{ph,2}, r_{ph,3} \right\} f_{w/b} \beta_H e^{\left(\frac{E_i}{R} \left(\frac{1}{I_0 - I}\right)\right)} \right) dt$$
 (1)

where A_{ph} (m²/kg) is the surface area of the clinker and fly ash, A_o (m²/kg) is the reference surface area, T (K) is the modeling temperature, T_o (K) is the reference temperature (298.15 K), E_i (J/mol) is the activation energy of each phase, R (8.314 J/mol-K) is the universal gas constant, and $r_{ph,1}$, $r_{ph,2}$ and $r_{ph,3}$ are the rates of nucleation and precipitation, diffusion, and the slowing of transport of dissolved species, respectively, as follows:

$$r_{ph,1} = \frac{K_{ph,1}}{N_{ph,1}} \left[1 - \alpha_{ph}(t) \right] - \ln \left[1 - \alpha_{ph}(t) \right]^{1 - N_{ph,1}}$$
 (2a)

$$r_{ph,2} = \frac{K_{ph,2}\sqrt[3]{\left(1-\alpha_{ph}(t)\right)^2}}{1-\sqrt[3]{1-\alpha_{ph}(t)}}$$
 (2b)

$$r_{ph,3} = K_{ph,3(1-\alpha_{ph}(t))^{N_{ph,3}}}$$
 (2c)

The constants $K_{ph,1}$, $K_{ph,2}$, $K_{ph,3}$ and $N_{ph,1}$ and $N_{ph,3}$ in Equations (2a)-(2c) are empirical parameters which are used to calculate the reaction rate expressions of respective phases. These coefficients were fit from dissolution studies of OPC clinker phases and fly ash, as described in Section 3. The original PK model contains $K_{ph,1}$, $K_{ph,2}$, $K_{ph,3}$ and $N_{ph,1}$ and $N_{ph,3}$ parameters for four phases. The MPK model contains $K_{ph,1}$, $K_{ph,2}$, $K_{ph,3}$ and $N_{ph,1}$ and $N_{ph,3}$ for seven phases and oxides. Section 3 describes the numerical process for used to determine these coefficients for the MPK model in more detail.

The factor that incorporates the influence of water-to-binder ratio (w/b) in equation 1a, $f_{w/b}$, is given as:

$$f_{w/b} = \left(1 + 3.33 \times \left(H \times \frac{w}{b} - \alpha_t\right)\right)^4 \text{ for } \alpha_t > H \times w / b$$
 (3)

where H is a fitting factor added to the original PK model by Lothenbach in Ref. [1], and is calculated using the methods described in Section 3.1. H is a term used in the calculation of $f_{w/b}$ which accounts for the

reduction of the rate of reaction at later ages, particularly when w/b is low. The term α_t refers to the average system degree of reaction at time t. The total system degree of reaction is taken as a weighted average for all phases and oxides.

The lowest value of $r_{ph 1,2.3}$ at time t is considered the rate controlling step for dissolution for the respective phase at time t. The MPK model computes a degree of reaction $\alpha_{ph}(t)$ for each of the seven components at that time, as well as an overall system degree of reaction, which is the weighted average of the degrees of reaction of each of the seven phases. Note that in the original PK model, the overall degree of reaction is the weighted average of the degree of hydration of the four clinker phases. Including the amorphous fly ash phases in the model means that the overall system degree of reaction is proportionally impacted by the replacement of the four OPC clinker phases by amorphous fly ash oxides. Hence, the average system degree of reaction (and mass of each dissolved phase) at time t of a system using the PK model will be different than that calculated using the MPK model. As a result, the acceleration or retardation of the reactions by the amorphous fly ash will be captured. Other fly ash and cement oxides are allowed to dissolve in proportion to the average system degree of reaction.

Finally, the effect of relative humidity on the degree of reaction is for the relative humidity (h)

$$\beta_H = \left[\frac{h - 0.55}{0.45} \right]^4 \tag{4}$$

In this work β_H is assumed to be 1 for saturated conditions.

In the present work, the DoR_{ph}^* must be either measured or estimated for a given fly ash. Thus, the DoR_{ph}^* of the three individual fly ash glass oxides (amorphous SiO_2 , Al_2O_3 , and CaO) must be obtained from quantitative x-ray diffraction (QXRD) or scanning electron microscopy electron dispersive X-ray spectroscopy (SEM-EDS) [25]. Total amorphous content in fly ashes can range between 20 and 100%, though it is typically between 50 and 80% for most conventional US fly ashes [31, 41]. Furthermore, the amorphous to bulk ratio of each individual oxide will vary within a single ash [45]. To this end, QXRD or SEM-EDS measurements are the most reliable way to measure DoR_{ph}^* .

3. Methods

3.1. Determination of fitting parameters for the MPK model – data sources

To calculate the fitting parameters (K $_{ph,1},\ K_{ph,2},\ K_{ph,3},\ N_{ph,1},\ N_{ph,3}$ and H) used to model dissolution rates for the MPK model, empirical measurements of the dissolution of amorphous SiO2, amorphous CaO, and amorphous Al₂O₃ over time were obtained from dissolution and reaction studies of two calcareous fly ashes reported in literature by Durdzinski et al. [31]. It is important to note that the model is calibrated using only two fly ash studies because, to the best knowledge of the authors, these are the only known sources of measured time-dependent dissolution data for individual fly ash glass phases for periods of over 4 days. While one prior modeling study did investigate dissolution rates of individual glass phases, this was accomplished via estimates from dissolution tests, and fly ash reactions were modeled as a composite, not based on measured individual glass oxide dissolution rates [17]. As additional dissolution data for fly ash glasses becomes available, the provisional empirical coefficients in the MPK model can be recalculated using the methods described in Section 3.2.

The w/b and fly ash mass replacement level used for the two fly ashes by Durdzinski et al. were 0.50, and 45%, respectively. The determination of the degree of reaction of the fly ash glassy phase assemblages were quantitatively determined by Durdzinski et al. using an innovative quantification method [43] using a combination of XRD and SEM-EDS and a novel clustering algorithm to characterize the amorphous phases. The initial bulk chemical composition of the two fly ashes is shown

in Table 1. The crystalline phase composition is shown in Table 1 and the oxide composition of the amorphous content is shown in Table 2. Table 3 shows the dissolved amount of each glassy oxide at different ages between 1 and 365 days. To obtain the glassy phase composition based on individual oxides, a weighted average of the oxides in each glass was used. Durdzinski et al. [31] report the glass composition for each fly ash glass group in the original work (Table 2), and these values were used for the weighting.

It should be noted that in Ref. [31] the fly ash glass oxides were grouped into 4 groups of glass phases. Each glass phase was comprised of different proportions of CaO, SiO2, and Al2O3. For purposes of the present work, the fly ash glass oxides were separated out from these four groups, and analyzed individually (as oxides). Although these oxides tend to be found in polymerized glass networks in fly ash, rather than as individual oxides, the reason for analyzing these data as oxides rather than glass groups as done in Ref. [31] was two-fold: First, given the broad heterogeneity and variability of fly ashes, the proportion of oxides in the glass groupings delineated in Ref. [31] may not describe other fly ash systems. Second, the MPK model is intended to provide inputs for thermodynamic modeling. The thermodynamic modeling algorithm (GEMS) uses the Gibbs Free Energy Minimization technique, which breaks out the inputs into their atomic forms to determine thermodynamically feasible equilibrium speciation that are defined in the CEM-DATA database [4]. Therefore, the MPK model was fit based on the fly ash glass oxides rather than using specific fly ash glass groups (such as those in Ref. [31]) which are not contained in the relevant thermodynamic libraries.

3.2. Determination of fitting parameters for the MPK model – model fitting

A nonlinear programming technique was employed to determine the empirical reaction rate coefficients of the MPK model. A damped least squares method (Levenberg-Marquardt) [46] was used to fit the parameterized function (i.e. the MPK equations) to the sets of measured data shown in Table 3. The fitting algorithm operates by iteratively reducing the sum of the square of the errors between the measured data and the parameterized function by sequentially updating the parameter values. Two minimization methods are used by Levenberg-Marquardt: Gauss-Newton [47] and gradient descent [48]. In the former case, the

Table 1Bulk composition and crystalline phase composition (all amounts in weight %) of the two studied fly ashes reported in Ref. [31].

	FA-1	FA-2
Al ₂ O ₃	19.8	18.2
SiO ₂	42.3	33.6
CaO	20.7	26.5
Na ₂ O	0.3	1.9
K ₂ O	1.5	0.4
MgO	2.2	6.4
Fe_2O_3	8.2	6.4
SO_3	1.4	2.2
TiO ₂	0.7	1.3
P_2O_5	0.3	0.9
CaSO ₄	1.8	2.0
Sum	97.2	97.7
C ₃ S	_	-
C_2S	2.5	0.5
C ₃ A	2.0	4.0
C ₄ AF	1	1.5
Quartz	1.3	3.5
Mullite	_	-
Dolomite	_	-
Calcite	_	-
Periclase	_	2.0
Gypsum	-	-
Amorphous	89.7	85.9

Table 2
Glass composition (weight percent) of FA-1 and FA-2 reported in Ref. [31].

	CaO (%)	SiO ₂ (%)	Al ₂ O ₃ (%)
FA-1 Si	2.9	83.2	7.4
FA-1 Ca-Si	26.5	41.7	19.5
FA-1 Al-Si	9.1	52.7	25.5
FA-1 Ca-Al-Si	44.4	29.2	14.4
FA-2 Si	3.1	89.2	1.9
FA-2 Ca-Si	27.6	41.5	13.2
FA-2 Al-Si	9.1	45.8	30.0
FA-2 Ca-Al-Si	39.4	18.9	20.8

Table 3Dissolved amount of each glassy oxide (g/100 g binder) at different ages between 1 and 365 days from Refs. [31].

Day	FA-1 (g	dissolved)		FA-2 (g	FA-2 (g dissolved)			
	CaO	Al_2O_3	SiO_2	CaO	Al_2O_3	SiO_2		
1	0.64	1.07	1.90	1.62	0.85	1.93		
7	1.66	2.85	5.22	5.98	3.15	4.40		
28	2.47	4.17	7.74	7.54	4.35	6.34		
56	2.85	4.75	8.87	7.87	4.85	7.36		
90	3.07	5.10	9.55	8.01	5.12	7.94		
365	3.55	5.86	11.03	8.15	5.40	8.89		

sum of the squared errors is reduced by assuming a locally quadratic least squares function and finding the minimum of the quadratic. In the latter case, the errors are reduced by updating parameters iteratively in the steepest descent direction. In solving the optimization problem, the algorithm behaves like Gauss-Newton as the parameters near their optimal value, and like the gradient-descent method when the solution is far from optimal. The Levenberg-Marquart algorithm was selected in this study because it overcomes the disadvantages of either a purely Gauss-Newton method or purely gradient descent method (i.e. parameter evaporation or inaccuracy of results for moderately complex functions and slow convergence, respectively). The accuracy of the results of the algorithm were evaluated by both observing the sum of the square of the errors between the experimental and fitted data, and by comparing the results of the MPK equations using the coefficients produced from the fitted data, to the predicted dissolution-reaction data shown in Table 3. The results are described in Section 4.1.

3.3. Validation of the MPK model

The MPK model is validated based on a combination of independent dissolution data in OPC/amorphous silica systems, and on thermodynamic data for multiple OPC/fly ash systems. First, the amorphous SiO_2 coefficients were compared to those calculated for OPC/amorphous silica systems. Next, the empirical coefficients calculated for the amorphous SiO_2 in the fly ashes were bootstrapped to calculate the dissolution rates of amorphous SiO_2 in additional OPC/amorphous silica systems (and compared to experimental measurements of the same). Finally, the MPK model was applied to provide the kinetic inputs for thermodynamic modeling, and solid reaction products as well as pore solution chemistry were simulated and compared to both experimental measurements, as well as other theoretical approaches.

4. Results and discussion

4.1. Empirical parameters

The empirical reaction rate parameters obtained from the optimization algorithm described in Section 3 are shown in Table 4, along with the sum of the square of the errors obtained, and the $\rm R^2$ value of the fit between the reproduced model and experimental data.

Given the ability of the fitted model coefficients and equations to

Table 4 Empirical reaction rate coefficients for the MPK model; and the R^2 of the fit between the model results and experiment.

	K_1	N_1	K_2	K_3	N_3	Н	R^2
SiO ₂ (FA-1)	0.490	0.630	0.047	0.042	3.978	1.340	0.99
SiO ₂ (FA-2)	0.490	0.621	0.047	0.682	3.977	1.340	0.99
SiO ₂ [27]	0.490	0.621	0.050	0.389	3.426	0.040	
SiO ₂ [27]	0.492	0.636	0.043	1.291	3.142	1.440	
SiO ₂ (average)	0.490	0.626	0.047	0.362	3.988	1.040	
CaO (FA-1)	1.000	1.700	2.000	0.338	0.987	0.010	0.99
CaO (FA-2)	1.000	1.700	2.000	0.140	0.973	0.010	0.95
CaO (average)	1.000	1.700	2.000	0.239	0.980	0.010	
Al_2O_3 (FA-1)	0.501	0.704	0.050	0.065	2.000	0.090	0.99
Al_2O_3 (FA-2)	0.499	0.699	0.050	0.721	1.999	0.090	0.99
Al ₂ O ₃	0.500	0.702	0.050	0.393	2.000	0.090	
(average)							

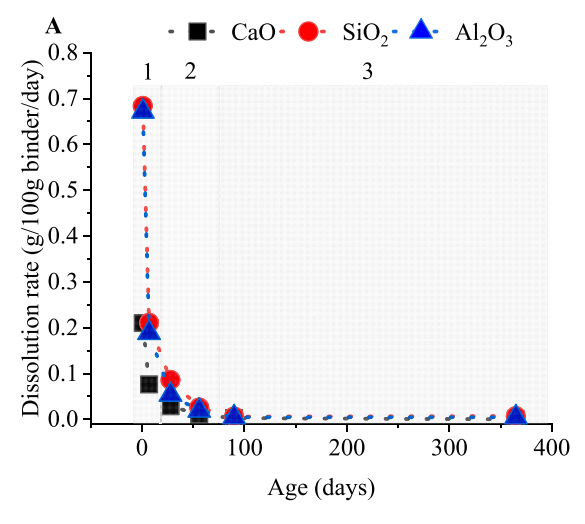
reproduce experimental values (as demonstrated by the R² values in Table 4), the arithmetic mean of the empirical parameters should be used for modeling. The data shown in Table 4 demonstrate that the MPK model can accurately reproduce the experimental results obtained by Durdzinski et al. [31], however independent validation of the model is necessary to ensure its broader applicability as described later in Section 4.3 - 4.5. First the results of the optimization problem are discussed.

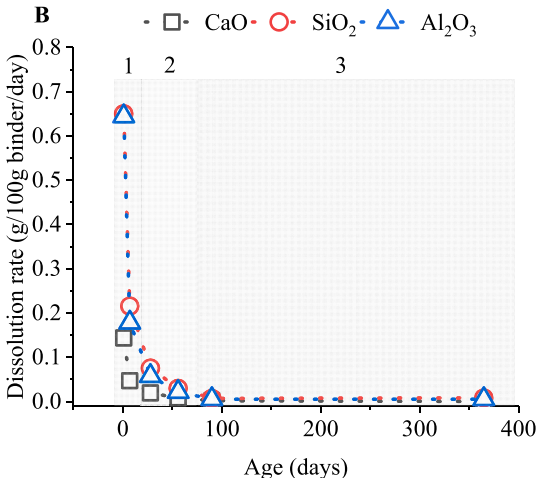
4.2. Comparison of dissolution-reaction kinetics for CaO, Al_2O_3 , and SiO_2

It is instructive to consider the similarities and differences in dissolution-reaction kinetics between the three major fly ash oxides in this study: (amorphous) CaO, Al₂O₃, and SiO₂. CaO, Al₂O₃, and SiO₂ are known to behave differently from one another in cementitious mixtures due in part to their charge (and therefore binding capacity), and in part due to their pozzolanic versus hydraulic nature [30]. SiO2 and Al2O3 are primarily pozzolanic in nature [49], whereas CaO contributes to hydraulic properties [50]. Therefore, it is expected that differences in dissolution and reaction rates may be observed between these three oxides. Table 4 provides the empirical coefficients calculated for the pozzolanic oxides (Al₂O₃ and SiO₂) and shows that these values are somewhat similar to each other; however, they are different than those calculated for CaO. The K1 and N1 parameters which belong to the nucleation/precipitation equation for CaO are \geq 1.0, but <1.0 for Al $_2$ O $_3$ and SiO_2 . For the K_2 values, which are associated with the diffusion equation, CaO is 2.0 and Al₂O₃ and SiO₂ are each <1.0. This is indicative of the slower dissolution rate of calcium. This is discussed in more detail in the paragraph below.

Fig. 1 shows the modeled (Fig. 1A) and measured (Fig. 1B) dissolution rates of the individual oxides and a scatter plot of modeled versus experimental dissolution rates (Fig. 1C). The data in Fig. 1B are the same data as those reported in Ref. [31], however, in Ref. [31] the fly ash oxides were grouped into four groups of glass phases comprised of different proportions of each of these oxides, and here, they oxides are broken out from these larger four groups of glasses for purposes of analysis. Transposed onto Fig. 1A and B are the approximate points in the reaction process where nucleation and precipitation (Equation (2a)); diffusion (Equation (2b)); and reduction in rate of ionic transport (Equation (2c)) are the rate limiting factors. Determining which of these reactions are rate controlling at which time depends on (among other things) mixture composition, temperature, fly ash replacement amount, and particle size [51]. These results are consistent with earlier work, which has shown that nucleation and precipitation begins at the time of initial mixing [16,52], and that diffusion and reduction of rate of ionic transport are the rate controlling steps for the majority of the later reaction process [16].

Several observations can be drawn from these plots. The first observation is that the modeled (A) and measured (B) rates are nearly identical (Fig. 1C). This is expected, and is also reflected in the





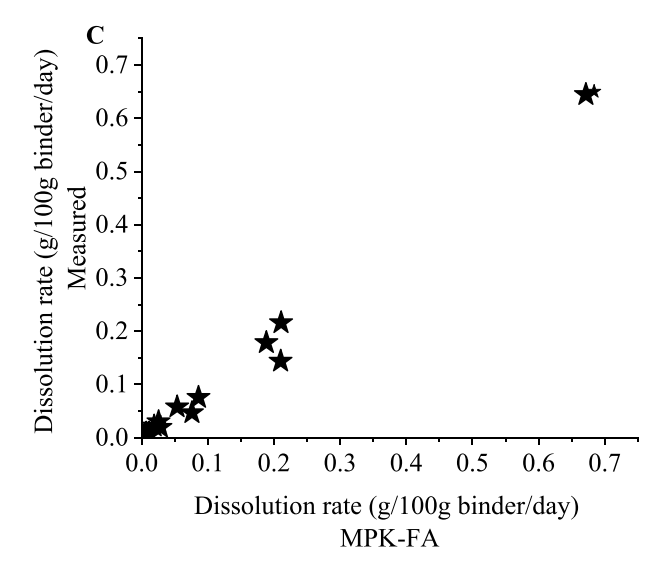


Fig. 1. Dissolution rates of the individual oxides A. modeled; and B. measured. Dashed lines do not represent actual data and are for ease of viewing only. Transposed onto the figures are the approximate stages of the dissolution precipitation process: 1) nucleation/precipitation; 2) diffusion; 3) reduction in transport. Fig. 1C shows the measured and modeled dissolution rates plotted against each other for ease of comparison.

correlations reported in Table 4. Another observation is that the reaction rates shown are reflective of those found in literature [3,53]. For each oxide, early-age reaction rates (1–7 days) are substantially higher than later-age reaction rates, and after an initial rapid reduction, slow down and asymptotically approach zero. These results may also be contextualized by other experimental and modeling investigations which have found that around 90 days, the reactivity of many fly ashes tends to plateau or slow significantly after this time [17].

Another noteworthy observation from this figure is that the early dissolution rate of CaO is considerably lower than that of SiO2 and Al₂O₃. At all ages, the dissolution rate of SiO₂ is slightly faster than Al₂O₃, and the dissolution rate of CaO is slower than both; although at later ages, the difference between the dissolution rates of the oxides narrows. Specifically, 1-day SiO₂ and Al₂O₃ dissolution rates are roughly 0.6 g/100 g binder/day, whereas the 1-day dissolution rate of CaO is roughly 3 times lower at 0.2 g/100 g binder/day. At 7 days, the SiO₂ and Al₂O₃ dissolution rates are an order of magnitude higher than CaO: roughly 0.20 g/100 g binder/day versus 0.05 g/100 g binder/day for CaO. After 90 days the dissolution rates of all three oxides tend to slow down substantially and converge with one another, although the dissolution rate of calcium is still notably slower than either SiO2 or Al₂O₃ at 1 year. At 365 days, the SiO₂ and Al₂O₃ dissolution rates are 0.005 g/100 g binder/day, and the CaO dissolution rate is roughly 0.002 g/100 g binder/day.

Prior experimental work has found that fly ashes rich in amorphous SiO₂ and Al₂O₃ react faster than CaO rich fly ashes, and that Al and Si tend to dissolve congruently, whereas calcium dissolution is hindered in mixtures above a 1.0 M CaO/Al₂O₃ molar ratio, which corresponds to a nearly fully condensed glass network structure [54]. While past work has demonstrated that calcium can accelerate the dissolution of aluminosilicates, the reaction of the calcium itself appears to be slower. In other words, the presence of calcium in a glass structure can accelerate the dissolution of Al₂O₃, but not vice versa [53]. In a glass containing Ca, Si, and Al, the calcium acts as a network modifier in the glass structure, and is bound ionically (unlike the Si and Al which are covalently bonded), thus making the glass structure vulnerable to attack by aqueous ionic solutions [53]. Another potential explanation for the slower dissolution of CaO is the supersaturation of pore solution from calcium rich clinker phases, which would limit the dissolution of calcium from the fly ash [55,56].

4.3. Comparison of amorphous SiO₂ dissolution in silica fume and fly ash

As a preliminary cross-validation of the MPK model to earlier works, the reaction rate coefficients for amorphous SiO_2 calculated for the present work are compared to the reaction rate coefficients for amorphous SiO_2 calculated in prior work [27]. These results are shown in Table 4. It is expected that if amorphous silica in fly ash behaves similarly to that of the amorphous silica in silica fume, then the empirical parameters should likewise be similar. Although experimental work is limited, past work has demonstrated that the amorphous silica in fly ash dissolves at a similar rate to amorphous silica in silica fume [3,7], and similarly shifts the overall system degree of reaction to earlier ages.

As seen in Table 4, the empirical parameters calculated from the present work for fly ash are nearly identical to those calculated for silica fume. This indicates that the overall dissolution-reaction kinetics for the amorphous silica in fly ash is similar to the amorphous silica in silica fume as found in the prior works [27]. In addition, these results suggest that the MPK model is able to accurately capture the dissolution kinetics of amorphous ${\rm SiO}_2$ in fly ash. The similarity in the empirical coefficients in models, therefore, provides promising cross-validation of the kinetic behavior of amorphous silica to both prior models and prior experimental evidence.

4.4. Using the MPK empirical coefficients for amorphous SiO₂ to bootstrap measured dissolution in OPC/amorphous SiO₂ systems

While the ultimate purpose of the MPK model is to provide the numerical input necessary for thermodynamic modeling OPC/fly ash systems at non-equilibrium conditions, it must first be demonstrated that the model can accurately predict the dissolution rates in other, independent systems. Since no other known time-dependent experimental dissolution data for fly ash glasses exist, dissolution data for amorphous silica as determined by ²⁹Si MAS NMR were obtained from two additional, separate studies by Muller et al. [57] and Lothenbach et al. [58]. In the first study by Muller et al. [57] amorphous SiO₂ dissolution was measured at 3, 7, 14, and 28 days. The w/b of the system studied by Muller et al. was 0.40, and the silica fume was comprised of 98.6% amorphous SiO_2 with a specific surface area of 20 m²/g. The silica fume mass replacement level was 10%. Using the average of the amorphous SiO₂ empirical coefficients (Table 4), the MPK model was run using the materials and test conditions in Muller et al. An R² of 0.99 was obtained. In the second separate independent study from Lothenbach et al. [58] for a low alkali cement with a 10% mass replacement of silica fume comprised of 99.8% amorphous nanosilica and a w/b of 1.1. The MPK model was run using the average of the empirical coefficients (Table 4). An R² of 0.99 was obtained.

4.5. Thermodynamic validation

Sections 4.1-4.4 demonstrate that the MPK model accurately predicts the following:

- The dissolution rates and overall dissolved masses of the experimental studies used to fit the model;
- The dissolution rates of amorphous silica as compared to prior dissolution models and studies; and
- 3. The relative and absolute dissolution rates of amorphous Ca, Si, and Al as compared to general values reported in literature.

The following sections show the results of the MPK model compared to prior experimental studies. In the present work, the curing conditions for the pastes used to calibrate the model was 20 °C, and the curing conditions of the pastes used to validate the model were 20 °C. Although it is expected that like the PK model, the MPK model should apply to pastes cured at different temperatures, insofar as the equation has a term to account for initial temperature, and insofar as the subsequent thermodynamic calculations may also be adjusted based on the temperature used in the MPK model and/or test system, future work will further verify this by evaluating pastes cured at accelerated temperatures.

In addition, the MPK model is compared to a commonly used theoretical approach in modeling which uses the PK model and a measured or assumed maximum overall degree of reactivity of the fly ash (PK + reactivity), where the fly ash oxides all dissolve uniformly [8].

As described above, the MPK model provides the kinetic inputs for thermodynamic modeling at non-equilibrium conditions. The kinetic inputs from the MPK model are entered in the form of grams of each of the seven OPC phases and fly ash oxides dissolved at either different ages or different average system degrees of reaction. Other minor cement oxides are allowed to dissolve proportionally to the overall average system degree of reaction at the age of interest.

Thermodynamic modeling is performed using the GEMS3K [59] algorithm, the CemData 18.1 database [4], and associated software developed by the authors of this study. GEMS3K uses a Gibbs Energy Minimization algorithm to compute the equilibrium phase assemblage and speciation in cementitious systems based on the bulk elemental compositions and pressure and temperature [60]. Thermodynamic equilibrium of a system is achieved when the spontaneous energy of the system is at a minimum. In GEMS3K, equilibrium composition of the whole system is found from all of the possible stoichiometric

combinations of the phases. A benefit of the GEMS3K approach is that no a priori assumptions need to be made regarding the phases, the solid solution composition, the solution pH, redox potential, or fugacity of gasses [4]. These values are computed as outputs from the GEMS3K algorithm. A limitation of GEMS3K however, is that in order to produce accurate results, the inputs to the software must reflect the bulk chemical composition of the system as it approaches equilibrium. The reactions that occur while cement and fly ash hydrate and react however, are implicitly transient [5,44]. Both the rates of reaction and the masses of the bulk independent components of the system are kinetically constrained [9]. To this end, the MPK model provides a framework from which these kinetic values can be reliably calculated for almost any OPC/fly ash mixture, and inputted into GEMS3K as "quasi-equilibrium" values to enable thermodynamic calculations of the systems at non-equilibrium conditions.

4.5.1. Solid reaction products - calcium hydroxide

Calcium-hydroxide (CH) amounts for several fly ash/OPC mixtures were obtained from literature. In one such study, Kucharczyk et al. [61] synthesized eight different CaO-Al2O3-SiO2 glasses, seven of which represented typical fly ash compositions, and the other was a synthetic slag. The seven fly ash compositions are shown in Table 5. The slag was not used in the present study since it is outside the scope of the model. Experiments were performed at a w/b of 0.50 and a mass replacement level of 45.2%. Chemical composition and other material properties used in the model can be found in the original study [61]. Since the fly ashes in this study were 100% reactive glass, the DoR_{ph}* of the CaO, SiO₂, and Al₂O₃ were 100%. This assumption would be highly inaccurate for a non-synthetic fly ash. The 100% value reflects the fact that the fly ash oxides are all amorphous; in a real fly ash this figure would be lower. It should be noted that a 100% fly ash reactivity is an extreme example, and not at all realistic for actual fly ashes. However, since the fly ashes from this study are all composed of synthetic and fully reactive glass, this simplified system allows for an uncomplicated comparison of a thermodynamic model with fly ash kinetics and without it (i.e. the MPK model). The MPK model was run using the experimental conditions of Kucharczyk et al. [65], and compared to both the experiment and to the PK + reactivity approach, where it was assumed that 100% of each fly ash is available for reaction at all ages. More realistic fly ash reactivity values are used to validate the MPK model in forthcoming sections. However, for this study containing synthetic and fully reactive ashes, Fig. 2 shows the results of the experiments, and of MPK versus PK + 100% reactivity approach.

From Fig. 2, two observations can immediately be made. The first is that the MPK model is in good agreement with the experiments. The second is that the PK + reactivity approach vastly overestimates the fly ash reactivity and its CH consumption, due to the fact that all of the pozzolanic phases in the fly ash are assumed to react immediately, resulting in the consumption of nearly all the CH in the system at 180 days. The only mixtures where any CH is predicted by PK + reactivity are those containing G3, G4, G6 and G7, all systems with initial SiO $_2$ amounts of 60% or less. For these four fly ashes, CH amounts are vastly underpredicted by 12%, 14%, 12%, and 11% respectively. In contrast the MPK model is always within 0–2% of the experimental values.

Table 5Chemical composition of the seven synthetic fly ashes glasses synthesized by Ref. [61].

	G1	G2	G3	G4	G5	G6	G7
Al ₂ O ₃ (%)	16.8	26.3	35.1	26.7	16.6	26.1	36.3
SiO ₂ (%)	78.5	69.1	60.6	59.4	62	49.8	39.7
CaO (%)	4.7	4.7	4.3	13.9	21.4	24.1	24.0
Sum (%)	100	100	100	100	100	100	100
Ca/(Al+Si)	0.05	0.05	0.04	0.12	0.27	0.32	0.31
Ca/Al	0.5	0.3	0.2	0.9	2.3	1.7	1.2
Al/Si	0.1	0.2	0.3	0.3	0.2	0.3	0.5

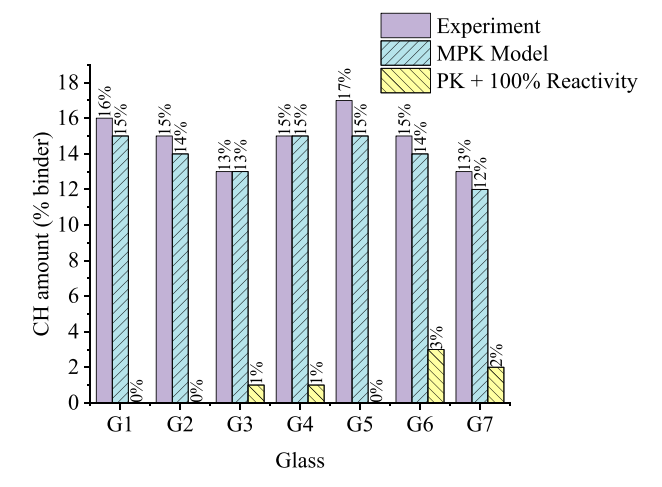


Fig. 2. CH amounts at 180 days for the seven synthetic fly ash and cement pastes [61], compared to the results of the MPK based thermodynamic simulations, and the PK+ reactivity thermodynamic simulations.

In addition to the synthetic fly ashes modeled above, CH amounts were also modeled for the fly ashes reported by de Weerdt et al. [18] using both the MPK model and the PK + reactivity approach. From this study, CH amounts, given as a percent of binder, were obtained for the pastes at different ages. The w/b of the pastes in this study was 0.50 and the fly ash mass replacement was 35%. Material and experimental conditions are reported in the original study [18]. For the PK + reactivity modeling approach, two different fly ash reactivities were modeled: first, the fly ash reactivity was modeled at 68% to reflect the 68% amorphous content of the ash (68% of the fly ash phases were modeled as uniformly dissolved at all ages), as would have been done using earlier thermodynamic approaches [8]. The fly ash was also modeled at a reactivity of 25%, which reflects the approximate mean value of maximum degree of reaction for American fly ash obtained from multiple publications [24,36,62-67] (25% of the fly ash phases were modeled as dissolved at all ages). In neither PK + reactivity approach was fly ash kinetics incorporated.

For the MPK model, the DoR_{ph}^* of the fly ash oxides reflect the proportion of each individual oxide that was amorphous as determined by subtracting the crystalline phases determined by QXRD from the bulk composition. Results shown in Fig. 3 are consistent with those from Fig. 2 – the MPK model closely predicts the experimental data, however,

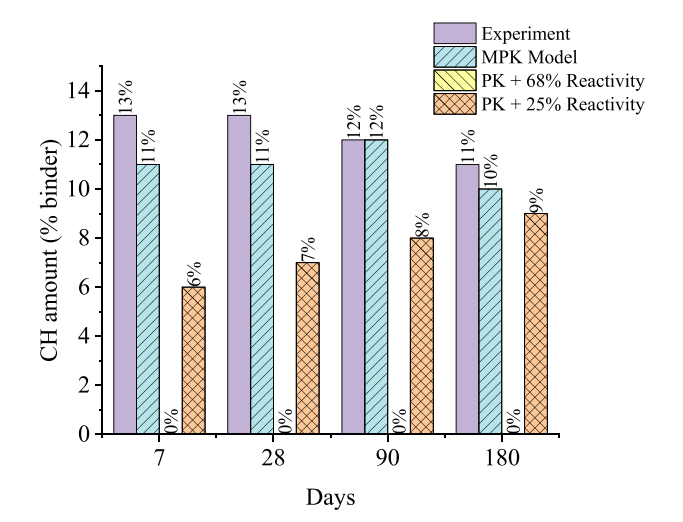


Fig. 3. CH amounts expressed as a percent of binder from 7 to 180 days as compared to the results [18], MPK based thermodynamic simulations, and the PK+ reactivity thermodynamic simulations.

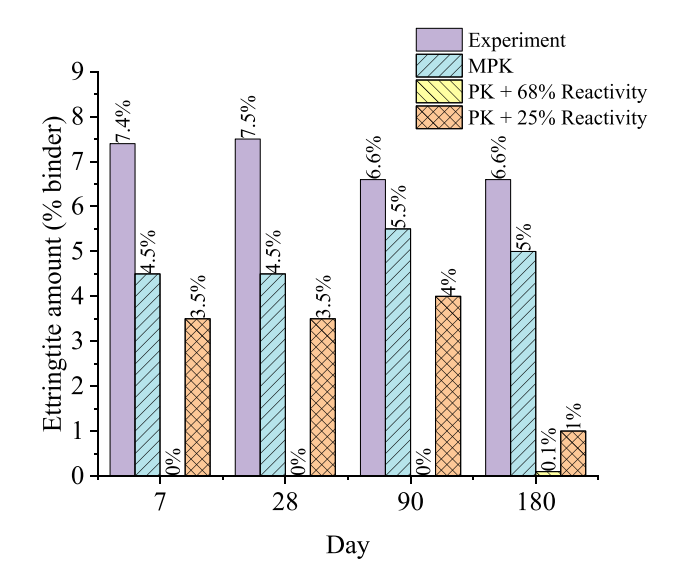


Fig. 4. Ettringite amount expressed as a percent of binder from 7 to 180 days as compared to the results of the experiments [18], and MPK based thermodynamic simulations, and the PK+ reactivity thermodynamic simulations.

the PK + reactivity model does not. In the PK + 68% reactivity model, the proportion of binder that is CH is always 0% at all ages, which is a consequence of the high silica content of this ash, and the model assumption that it is always dissolved in solution. In the PK + 25% reactivity approach, CH amounts are predicted to be between 6 and 9% of the binder at different ages. Although the PK + 25% reactivity model has a much higher error than the MPK model (underpredicting CH by roughly to 50% of experimental values at early ages) it becomes more accurate as the system approaches true equilibrium at 180 days. This is a consequence of the fly ash reaction being immediately completed in the PK + 25% approach, since there is no kinetic restriction on dissolution rate. Following the complete reaction of the fly ash, the continuous hydration due to cement-only kinetics results in an increased CH content. It is apparent that even using an arbitrarily average reactivity value in the PK + reactivity approach, the progression of reactions and reaction pathways are not captured, and early age modeling of the reactions is inaccurate. In contrast, the MPK model predicts early age CH amounts within 2% of the binder amount (15% of experimental values) at early ages, reflecting its ability to capture the early age dissolution and reaction of the fly ash phases. At 90 days, the MPK model exactly matches the experimental measurements, and at 180 days, matches within 1% of binder (see Fig. 4).

4.5.2. Solid reaction products – ettringite

To further validate the MPK model, ettringite amounts (percent of binder) were also modeled using the MPK approach and compared to the data reported by de Weerdt et al. [18]. As with CH, the results of the MPK model and experiments are compared to the PK + reactivity approach for reaction extents of 68% and 25%. As noted in the study by de Weerdt et al. [17], the presence of fly ash in the OPC results in higher amounts of ettringite formed than in plain OPC systems [18]. The ettringite amounts as modeled by MPK compare favorably to the experimental results, predicting ettringite amounts in the binder within 1-3% of the experiments. In the PK + 68% reactivity model, almost no ettringite is formed, due to C-S-H comprising the bulk of the binder. In the PK + 25% reactivity model, ettringite amounts are predicted with less precision than the MPK model, particularly at late ages, where the model underpredicts the ettringite content in the binder by over 5%. This is in contrast with the CH predictions, which improved at later ages in the PK + 25% reactivity model. The reason for the poorer ettringite prediction at late ages in the PK + 25% reactivity model likely is related to the overprediction of pore solution pH (as discussed in Section 4.5.3),

and the inaccurate estimation of sulfate dissolution [68]. The thermodynamic stability of ettringite is generally low at both low and high pH values. While the exact pH at which ettringite will decompose is not well understood, generally pH values of lower than 12 and higher than 14 are associated with destabilization of ettringite [69,70].

4.5.3. Pore solution

Section 4.5.1 and 4.5.2 demonstrated that the MPK model is in good agreement with experimental measurements of solid hydration products. Since the pore solution is the reaction medium in cementitious systems, pore solution pH and compositions as predicted by MPK are compared to experimentally determined values. These values are further compared to a PK + reactivity modeling approach to demonstrate how the incorporation of kinetics is necessary to accurately predict these parameters.

The pore solution pH of the fly ash/cement reported by de Weerdt et al. [18] at different ages between 7 and 140 days is shown in Fig. 5. Consistent with prior findings, the presence of fly ash leads to a reduction in pH values (in the study of de Weerdt et al., the pH of a neat cement pore solution was also measured, and fell between 13.7 and 13.8 at all ages) [18]. For the OPC/fly ash mixtures, the pH decreases from 13.6 at 7 days, to 13.4 at 140 days. At early ages, the reduction in pH is likely due to dilution, but after 28 days, it is a consequence of the reduction in alkali concentrations in the pore solution, as they are incorporated into the solid hydration products [32]. The MPK model is able to accurately predict the pore solution pH within an accuracy of 0-0.01 pH units of the experiments. Furthermore, the MPK model captures the reduction in pore solution pH at later ages, whereas both the PK + 25% and PK + 68% reactivity model show a stable or increasing pH after 28 days. While the PK + 25% reactivity does perform better than PK + 68% reactivity, the values it predicts are still considerably off from experimental values. The likely reason for the high pH values predicted by the PK + reactivity approaches is that these models uniformly allow for full dissolution of the fly ash alkali hydroxides at all ages. This results in a greater overall mass of alkali being modeled as dissolved at all ages.

Major ionic species (Na $^+$, K $^+$, and OH $^-$) in the pore solution were modeled using the MPK and PK + 25% reactivity approach. These results are shown in Fig. 6A–C. The MPK model shows good agreement with the experimental results at all ages. With the exception of 7-day K $^+$ pore solution concentrations where predictions are identical to the PK + 25% reactivity model, the MPK is always more accurate than the PK + 25%

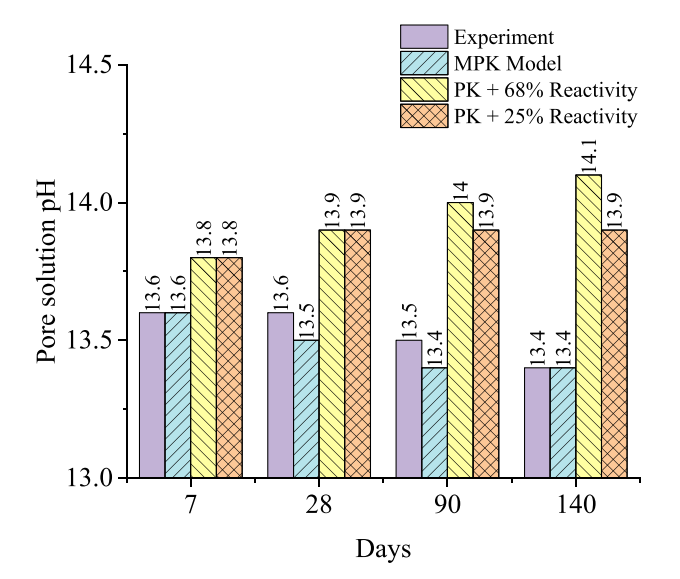
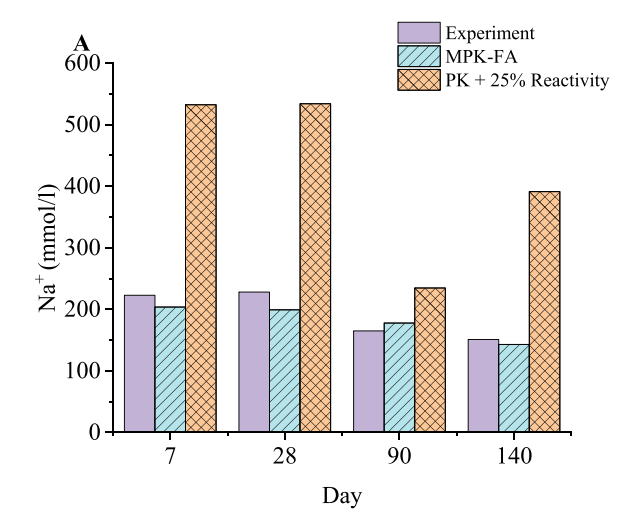
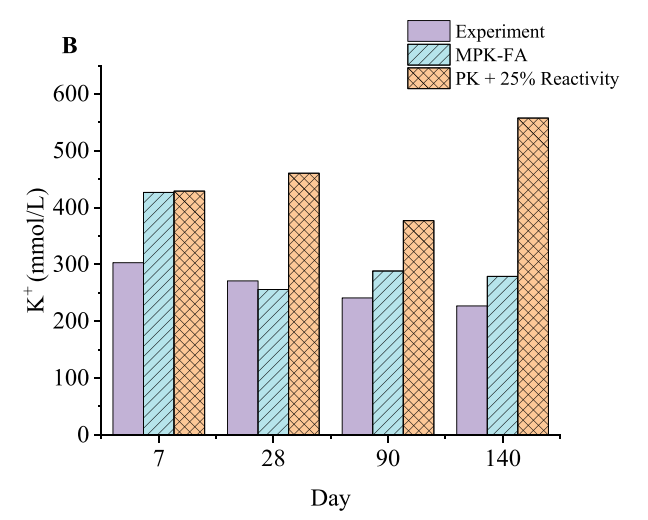


Fig. 5. Pore solution pH from 7 to 140 days as compared to the results of the experiments [18], and MPK based thermodynamic simulations, and the PK+ reactivity thermodynamic simulations.





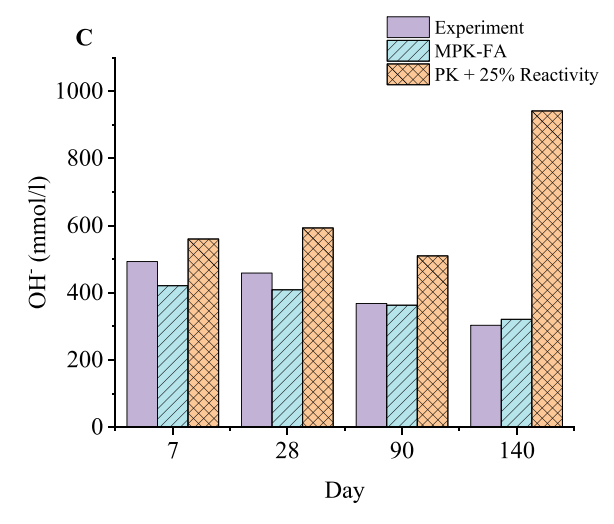


Fig. 6. Pore solution concentrations of A. Na^+ , B. K^+ , and C. OH^- from Ref. [18] for 7–140 days as compared to the results of experiments and MPK based thermodynamic simulations, and the PK + reactivity simulations.

reactivity approach, with the PK + 25% reactivity approach overestimating ionic concentrations by up to 300% (such as the 140-day OH $^-$) values. By way of contrast, the MPK model is typically within 5–10% of the experimental measurements. These results should be considered in the context of the pore solution pH predictions (Fig. 5): it is expected that with the accurate MPK pH predictions, the major ionic

species in the pore solution should be in good agreement with experiments, since pore solution ionic activity and pH are related.

Similar to CH predictions, which became slightly more accurate with age using the MPK model (Fig. 3), there is a trend of increasing accuracy in the pore solution composition as age increases using MPK. However, as with the CH predictions, the overall agreement is strong at all ages. It is interesting to note that the PK + 25% reactivity predictions tend to become less reliable at later ages for K^+ and OH^- , and more reliable for Na^+ , with the exception of the 90-day predictions, which most closely match the experimental measurements for each ion. It is likely that this is a consequence of the specific chemical composition of this OPC/fly ash mixture serendipitously matching the fractional amounts of the alkali concentrations used as inputs. In that sense, the improvement in 90-day agreement using PK + 25% reactivity results is rather arbitrary, and it is not expected that 90-day predictions would necessarily show improvement for mixtures with different compositions.

4.6. Limitations and future work

It has been demonstrated that the MPK model provides a reliable framework for predicting dissolution rates of major amorphous fly ash oxides, and that these dissolution rates can be used in conjunction with thermodynamic calculations to accurately predict time dependent reaction pathways and products for a range of OPC/fly ash mixtures. It should be noted that due to the newness and complexity involved with quantifying the dissolution rates of individual fly ash oxides, datasets from which to fit the empirical parameters are somewhat limited. To this end, the authors note that although a range of fly ash bulk and amorphous compositions have been tested and validated using this model, the datasets used to fit as well as validate the MPK model had the same w/b ratios (0.50) and similar fly ash replacement levels (35-45%). Therefore, future work is needed to further extend both the fitting as well as validation datasets for a wider range of w/b and fly ash replacement amounts, as these data become available. It is intended that the MPK framework should be further modified as experimental innovations increase the ease of producing these datasets. Furthermore, as the field matures with respect to quantifying the mechanisms and differences between glassy phase dissolution rates based on their composition and structure, and as thermodynamic data become available for the specific glass compositions and structures, the MPK model can be modified to model dissolution by glass composition and structure rather than amorphous oxide composition. However, in the absence of these data, the MPK model currently provides a reliable framework for determining the overall dissolution behavior of amorphous fly ash for a range of chemical compositions.

5. Conclusions

This paper describes the extension of a kinetic model, known as the modified Parrot-Killoh model for fly ash (MPK model) to include major fly ash glass oxides in cementitious mixtures. The model is based on the form of the Parrot-Killoh model which determines the reaction kinetics based on a rate limiting for various oxides and phases. The time dependent dissolution rates of seven major cement and fly ash phases and fly ash glass oxides (C3A, C3S, C2A, C4AF, SiO2, CaO, Al2O3) are determined using empirical coefficients that were fit from experimental measurements. These dissolution rates allow for determination of the mass of each phase dissolved at different ages, which can be used as inputs for thermodynamic modeling to estimate the proportion of each phase that is available for reaction at each stage in the hydration process. Experimental observations from the literature are compared with model predictions for solid hydration products (calcium hydroxide and ettringite), pore solution pH, and pore solution chemistry for several ordinary portland cement (OPC)-fly ash mixtures at various ages. The MPK model predicts the amount of CH in OPC/fly ash binders within 2% of experimental measurements, ettringite amounts within 3%, pore

solution pH within 1%, and major pore solution ionic concentrations within 0.10–70 mmol/l, at ages ranging from 7 to 180 days. This paper demonstrates the importance of including fly ash amorphous content versus bulk composition in a model for fly ash dissolution kinetics. The results show that incorporating the kinetics of fly ash based on dissolution rates into thermodynamic calculations leads to improved predictions in thermodynamic models. The MPK model be used as a framework for modeling OPC/fly ash kinetics using thermodynamics. It is intended that the coefficients fit in this study be recalculated as more experimental data become available, and that over time, the kinetic model equations may be updated with a more mechanistically based model when the data to do so becomes available.

Declaration of competing interest

The authors declare that they have no known competing financial interests or personal relationships that could have appeared to influence the work reported in this paper.

Acknowledgments

The authors gratefully acknowledge the financial support provided by ARPA-E, Energy Power Research Institute (EPRI), and National Science Foundation (Grant number NSF CMMI 1728358). Deborah Glosser would like to thank Dr. Russell Schwartz for his helpful consultation on nonlinear programming.

References

- B. Lothenbach, F. Winnefeld, Thermodynamic modelling of the hydration of portland cement, Cem. Concr. Res. 36 (2006) 209–226, https://doi.org/10.1016/j. cemconres 2005 03 001
- [2] V.J. Azad, O.B. Isgor, A thermodynamic perspective on chloride limits of concrete produced with SCMs, ACI SP 308 (2016) 1–18.
- [3] B. Lothenbach, D. Rentsch, E. Wieland, Hydration of a silica fume blended lowalkali shotcrete cement, Phys. Chem. Earth 70 (2014) 3–16, https://doi.org/ 10.1016/j.pce.2013.09.007.
- [4] B. Lothenbach, D.A. Kulik, T. Matschei, M. Balonis, L. Baquerizo, B. Dilnesa, G. D. Miron, R.J. Myers, Cemdata18: a chemical thermodynamic database for hydrated Portland cements and alkali-activated materials, Cement Concr. Res. 115 (2019) 472–506, https://doi.org/10.1016/j.cemconres.2018.04.018.
- [5] B. Lothenbach, Thermodynamic equilibrium calculations in cementitious systems, Mater. Struct. Constr. 43 (2010) 1413–1433, https://doi.org/10.1617/s11527-010-9592-x.
- [6] L.J. Parrott, D.C. Killoh, Prediction of cement hydration, Proc. Br. Ceram. Soc. 35 (1984).
- [7] F. Deschner, B. Lothenbach, F. Winnefeld, J. Neubauer, Effect of temperature on the hydration of Portland cement blended with siliceous fly ash, Cement Concr. Res. 52 (2013) 169–181, https://doi.org/10.1016/j.cemconres.2013.07.006.
- [8] D. Glosser, V. Jafari Azad, B. Isgor, J. Weiss, P. Surraneni, An extension of the Powers-Brownyard model to pastes containing supplementary cementitious materials, ACI Mater. J. 116 (2018) 205–216, submitted for publication.
- [9] K.L. Scrivener, P. Juilland, P.J.M. Monteiro, Advances in understanding hydration of Portland cement, Cement Concr. Res. 78 (2015) 38–56, https://doi.org/ 10.1016/j.cemconres.2015.05.025.
- [10] A.F. Voter, F. Montalenti, T.C. Germann, Extending the time scale in atomistic simulation of materials, Annu. Rev. Mater. Sci. 32 (2002) 321–346, https://doi. org/10.1146/annurev.matsci.32.112601.141541.
- [11] H. Manzano, A. Van Duin, S. Yip, M. Buehler, F. Ulm, R. Pellenq, The C-S-H gel formation understood by atomistic simulation methods, in: Ángel Palomo (Ed.), 13th International Congress on the Chemistry of Cement Proceedings, ICCC, 2011.
- [12] A.G. Kalinichev, R.J. Kirkpatrick, Molecular dynamics modeling of chloride binding to the surfaces of calcium hydroxide, hydrated calcium aluminate, and calcium silicate phases, Chem. Mater. 14 (2002) 3539–3549, https://doi.org/ 10.1021/cm0107070.
- [13] D. Hou, H. Ma, Y. Zhu, Z. Li, Calcium silicate hydrate from dry to saturated state: structure, dynamics and mechanical properties, Acta Mater. 67 (2014) 81–94, https://doi.org/10.1016/j.actamat.2013.12.016.
- [14] K. van Breugel, Numerical simulation of hydration and microstructural development in hardening cement-based materials. (II) applications, Cement Concr. Res. 25 (1995) 522–530, https://doi.org/10.1016/0008-8846(95)00041-A.
- [15] G. Ye, J. Hu, K. Van Breugel, P. Stroeven, Characterization of the development of microstructure and porosity of cement-based materials by numerical simulation and ESEM image analysis, Mater. Struct. Constr. 35 (2002) 603–613, https://doi. org/10.1617/13935.

- [16] J.J. Thomas, A new approach to modeling the nucleation and growth kinetics of tricalcium silicate hydration, J. Am. Ceram. Soc. 90 (2007) 3282–3288, https:// doi.org/10.1111/j.1551-2916.2007.01858.x.
- [17] T. Wang, T. Ishida, Multiphase pozzolanic reaction model of low-calcium fly ash in cement systems, Cement Concr. Res. 122 (2019) 274–297, https://doi.org/ 10.1016/j.cemconres.2019.04.015.
- [18] K. De Weerdt, M. Ben Haha, G. Le Saout, K.O. Kjellsen, H. Justnes, B. Lothenbach, Hydration mechanisms of ternary Portland cements containing limestone powder and fly ash, Cement Concr. Res. 41 (2011) 279–291, https://doi.org/10.1016/j. cemconres.2010.11.014.
- [19] K. Bharadwaj, D. Glosser, M.K. Moradllo, O.B. Isgor, W.J. Weiss, Toward the prediction of pore volumes and freeze-thaw performance of concrete using thermodynamic modelling, Cement Concr. Res. 124 (2019) 105820, https://doi. org/10.1016/j.cemconres.2019.105820.
- [20] E. Guillon, J. Chen, G. Chanvillard, Physical and chemical modeling of the hydration kinetics of OPC paste using a semi-analytical approach, Proceedings of the CONMOD'08 International RILEM Symposium on Concrete Modelling (2008) 155-172
- [21] J.H. Lee, D.M. Roy, B. Mann, D. Stahl, Integrated approach to modeling long-term durability of concrete engineered barriers in LLRW disposal facility, MRS Online Proceedings Library Archive 353 (1995) 881–889.
- [22] V. Jafari Azad, P. Suraneni, O.B. Isgor, W.J. Weiss, Interpreting the pore structure of hydrating cement phases through a synergistic use of the Powers-Brownyard model, hydration kinetics, and thermodynamic calculations, Adv. Civ. Eng. Mater. 6 (1) (2017) 1–16, https://doi.org/10.1520/ACEM20160038.
- B. Lothenbach, K.L. Scrivener, D. Hooton, B. Lothenbach, K. Scrivener, R.
 D. Hooton, Supplementary cementitious materials, Cement Concr. Res. 41 (2011) 1244–1256, https://doi.org/10.1016/j.cemconres.2010.12.001.
- [24] P.T. Durdziński, M. Ben Haha, S.A. Bernal, N. De Belie, E. Gruyaert, B. Lothenbach, E. Menéndez Méndez, J.L. Provis, A. Schöler, C. Stabler, Z. Tan, Y. Villagrán Zaccardi, A. Vollpracht, F. Winnefeld, M. Zając, K.L. Scrivener, Outcomes of the RILEM round robin on degree of reaction of slag and fly ash in blended cements, Mater. Struct. Constr. 50 (135) (2017), https://doi.org/10.1617/s11527-017-1002-1
- [25] D. Glosser, A. Choudhary, O.B. Isgor, W.J. Weiss, Investigation of the reactivity of fly ash and its effect on mixture properties, ACI Mater. J. 116 (4) (2019) 193–200, https://doi.org/10.14359/51716722.
- [26] S.N. Whatley, P. Suraneni, V.J. Azad, O. Burkan Isgor, J. Weiss, Mitigation of calcium oxychloride formation in cement pastes using undensified silica fume, J. Mater. Civ. Eng. 29 (2017) 4017198, https://doi.org/10.1061/(ASCE)MT.1943-5532-0002052
- [27] D. Glosser, Equilibrium and Non-equilibrium Thermodynamic Modeling of Pastes Containing SCM, PhD Thesis, Oregon State University, Civil Engineering, 2020.
- [28] L.Q. Ge, J.H. Tang, Z.T. Yao, X.S. Ji, P.K. Sarker, M.S. Xia, Y.Q. Xi, A comprehensive review on the applications of coal fly ash, Earth Sci. Rev. 141 (2014) 105–121, https://doi.org/10.1016/j.earscirev.2014.11.016.
- [29] P. Suraneni, J. Weiss, Examining the pozzolanicity of supplementary cementitious materials using isothermal calorimetry and thermogravimetric analysis, Cem. Concr. Compos 83 (2017) 273–278, https://doi.org/10.1016/j. cemconcomp.2017.07.009.
- [30] P.T. Durdziński, R. Snellings, C.F. Dunant, M. Ben Haha, K.L. Scrivener, Fly ash as an assemblage of model Ca-Mg-Na-aluminosilicate glasses, Cement Concr. Res. 78 (2015) 263–272, https://doi.org/10.1016/j.cemconres.2015.08.005.
- [31] P.T. Durdziński, M. Ben Haha, M. Zajac, K.L. Scrivener, Phase assemblage of composite cements, Cement Concr. Res. 99 (2017) 172–182, https://doi.org/ 10.1016/j.cemconres.2017.05.009.
- [32] R. Snellings, Solution-controlled dissolution of supplementary cementitious material glasses at pH 13: the effect of solution composition on glass dissolution rates, J. Am. Ceram. Soc. 96 (2013) 2467–2475, https://doi.org/10.1111/ iace 12480
- [33] T. Oey, C. Huang, R. Worley, S. Ho, J. Timmons, K.L. Cheung, A. Kumar, M. Bauchy, G. Sant, Linking fly ash composition to performance in cementitious systems, 2015 World Coal Ash Conference Proceedings (2015). https://pdfs.semant icscholar.org/be98/14f44f2683e683db207d67589fa52b75f315.pdf.
- [34] C. Li, Y. Li, H. Sun, L. Li, The composition of fly ash glass phase and its dissolution properties applying to geopolymeric materials, J. Am. Ceram. Soc. 94 (2011) 1773–1778, https://doi.org/10.1111/j.1551-2916.2010.04337.x.
- [35] K.L. Scrivener, B. Lothenbach, N. De Belie, E. Gruyaert, J. Skibsted, R. Snellings, A. Vollpracht, TC 238-SCM: Hydration and microstructure of concrete with SCMs: state of the art on methods to determine degree of reaction of SCMs, Mater. Struct. Constr. 48 (2015) 835–862, https://doi.org/10.1617/s11527-015-0527-4.
- [36] Q. Zeng, K. Li, T. Fen-Chong, P. Dangla, Determination of cement hydration and pozzolanic reaction extents for fly-ash cement pastes, Construct. Build. Mater. 27 (2012) 560–569, https://doi.org/10.1016/j.conbuildmat.2011.07.007.
- [37] G.V.P.B. Singh, K.V.L. Subramaniam, Quantitative XRD analysis of binary blends of siliceous fly ash and hydrated cement, J. Mater. Civ. Eng. 28 (2016) 04016042, https://doi.org/10.1061/(ASCE)MT.1943-5533.
- [38] R.P. Williams, A. Van Riessen, Determination of the reactive component of fly ashes for geopolymer production using XRF and XRD, Fuel 89 (2010) 3683–3692, https://doi.org/10.1016/j.fuel.2010.07.031.
- [39] K. De Weerdt, M. Ben Haha, G. Le Saout, K.O. Kjellsen, H. Justnes, B. Lothenbach, Hydration mechanisms of ternary Portland cements containing limestone powder and fly ash, Cem. Concr. Res. 41 (2011) 279–291, https://doi.org/10.1016/j. cemeonres.2010.11.014.
- [40] R. Snellings, Solution-controlled dissolution of supplementary cementitious material glasses at pH 13: The effect of solution composition on glass dissolution

- rates, J. Am. Ceram. Soc. 96 (2013) 2467–2475, https://doi.org/10.1111/jace.12480
- [41] G.V.P.B. Singh, K.V.L. Subramaniam, Method for direct determination of glassy phase dissolution in hydrating fly ash-cement system using x-ray diffraction, J. Am. Ceram. Soc. 100 (2016) 403–412, https://doi.org/10.1111/jace.14486.
- [42] E.H. Oelkers, General kinetic description of multioxide silicate mineral and glass dissolution, Geochem. Cosmochim. Acta 65 (2001) 3703–3719, https://doi.org/ 10.1016/S0016-7037(01)00710-4.
- [43] P.T. Durdzinski, C.F. Dunant, M.B. Haha, K.L. Scrivener, A new quantification method based on SEM-EDS to assess fl y ash composition and study the reaction of its individual components in hydrating cement paste, Cem. Concr. Res. 73 (2015) 111–122, https://doi.org/10.1016/j.cemconres.2015.02.008.
- [44] L.J. Parrot, D.C. Killoh, Prediction of cement hydration, Br. Ceram. Proc. 35 (1984) 41–53.
- [45] R. Dhole, M.D.A. Thomas, K.J. Folliard, T. Drimalas, Characterization of fly ashes for sulfate resistance, ACI Mater. J. 110 (2013) 159–168.
- [46] K. Levenberg, A method for the solution of certain non-linear problems in least squares, Q. Appl. Math. 2 (1944) 164–168, https://doi.org/10.1090/qam/10666.
- [47] S. Gratton, A.S. Lawless, N.K. Nichols, Approximate Gauss-Newton methods for nonlinear least squares problems, SIAM J. Optim. 18 (2007) 106–132, https://doi. org/10.1137/050624935.
- [48] S. Roweis, Levenberg-Marquardt Optimization, Notes, Univ. Toronto, 1996.
- [49] R. Snellings, Assessing, understanding and unlocking supplementary cementitious materials, RILEM Tech. Lett. 1 (2016) 50–55, https://doi.org/10.21809/ rilemtechlett.2016.12.
- [50] T. Ramlochan, M.D.A. Thomas, R.D. Hooton, The effect of pozzolans and slag on the expansion of mortars cured at elevated temperature: Part II: microstructural and microchemical investigations, Cement Concr. Res. 34 (2004) 1341–1356, https://doi.org/10.1016/j.cemconres.2003.12.026.
- [51] S. Bishnoi, K.L. Scrivener, Studying nucleation and growth kinetics of alite hydration using μic, Cement Concr. Res. 39 (2009) 849–860, https://doi.org/ 10.1016/j.cemconres.2009.07.004.
- [52] A.N. Christensen, N.V.Y. Scarlett, I.C. Madsen, T.R. Jensen, J.C. Hanson, Real time study of cement and clinker phases hydration, Dalton Trans. 8 (2003) 1529–1536, https://doi.org/10.1039/b301095n.
- [53] K.C. Newlands, D.E. Macphee, The reactivity of aluminosilicate glasses in cements-effects of Ca content on dissolution characteristics and surface precipitation, Adv. Appl. Ceram. 116 (2017) 216–224, https://doi.org/10.1080/ 17436753.2017.1299986.
- [54] J. Skibsted, R. Snellings, Reactivity of supplementary cementitious materials (SCMs) in cement blends, Cement Concr. Res. 124 (2019) 105799, https://doi.org/ 10.1016/j.cemconres.2019.105799.
- [55] R. Snellings, Surface chemistry of calcium aluminosilicate glasses, J. Am. Ceram. Soc. 98 (2015) 303–314, https://doi.org/10.1111/jace.13263.
- [56] H. Maraghechi, F. Rajabipour, C.G. Pantano, W.D. Burgos, Effect of calcium on dissolution and precipitation reactions of amorphous silica at high alkalinity, Cement Concr. Res. 87 (2016) 1–13, https://doi.org/10.1016/j. cemeonres.2016.05.004
- [57] A.C.A. Muller, K.L. Scrivener, J. Skibsted, A.M. Gajewicz, P.J. McDonald, Influence of silica fume on the microstructure of cement pastes: new insights from ¹H NMR relaxometry, Cement Concr. Res. 74 (2015) 116–125, https://doi.org/10.1016/j. cemeonres.2015.04.005.
- [58] B. Lothenbach, G. Le Saout, M. Ben Haha, R. Figi, E. Wieland, Hydration of a low-alkali CEM III/B-SiO 2 cement (LAC), Cement Concr. Res. 42 (2012) 410–423, https://doi.org/10.1016/j.cemconres.2011.11.008.
- [59] D.A. Kulik, T. Wagner, S.V. Dmytrieva, G. Kosakowski, F.F. Hingerl, K. V. Chudnenko, U.R. Berner, GEM-Selektor geochemical modeling package: revised algorithm and GEMS3K numerical kernel for coupled simulation codes, Comput. Geosci. 17 (2013) 1–24, https://doi.org/10.1007/s10596-012-9310-6.
- [60] B. Lothenbach, F. Winnefeld, Thermodynamic modelling of the hydration of Portland cement, Cement Concr. Res. 36 (2006) 209–226, https://doi.org/ 10.1016/j.cemconres.2005.03.001.
- [61] S. Kucharczyk, M. Zajac, C. Stabler, R.M. Thomsen, M. Ben Haha, J. Skibsted, J. Deja, Structure and reactivity of synthetic CaO-Al2O3 -SiO2 glasses, Cem. Concr. Res. 120 (2019) 77–91, https://doi.org/10.1016/j.cemconres.2019.03.004.
- [62] V. Kocaba, E. Gallucci, K.L. Scrivener, Methods for determination of degree of reaction of slag in blended cement pastes, Cement Concr. Res. 42 (2012) 511–525, https://doi.org/10.1016/j.cemconres.2011.11.010.
- [63] Y.M. Zhang, W. Sun, H.D. Yan, Hydration of high-volume fly ash cement pastes, Cement Concr. Compos. 22 (2000) 445–452, https://doi.org/10.1016/S0958-9465 (00)00044-5.
- [64] X. Feng, E.J. Garboczi, D.P. Bentz, P.E. Stutzman, T.O. Mason, Estimation of the degree of hydration of blended cement pastes by a scanning electron microscope point-counting procedure, Cement Concr. Res. 34 (2004) 1787–1793, https://doi. org/10.1016/j.cemconres.2004.01.014.
- [65] M.B. Haha, K. De Weerdt, B. Lothenbach, Quantification of the degree of reaction of fly ash, Cement Concr. Res. 40 (2010) 1620–1629, https://doi.org/10.1016/j. cemconres.2010.07.004.
- [66] M. Narmluk, T. Nawa, Effect of curing temperature on pozzolanic reaction of fly ash in blended cement paste, Int. J. Chem. Eng. Appl. 5 (31) (2014), https://doi. org/10.7763/ijcea.2014.v5.346.
- [67] F. Deschner, B. Münch, F. Winnefeld, B. Lothenbach, Quantification of fly ash in hydrated, blended Portland cement pastes by backscattered electron imaging, J. Microsc. 251 (2013) 188–204, https://doi.org/10.1111/jmi.12061.

- [68] K. De Weerdt, K.O. Kjellsen, E. Sellevold, H. Justnes, Synergy between fly ash and limestone powder in ternary cements, Cement Concr. Compos. 33 (2011) 30–38, https://doi.org/10.1016/j.cemconcomp.2010.09.006.
- https://doi.org/10.1016/j.cemconcomp.2010.09.006.

 [69] Y. Shimada, J.F. Young, Thermal stability of ettringite in alkaline solutions at 80°C, Cement Concr. Res. 34 (2004) 2261–2268, https://doi.org/10.1016/j.cemconres.2004.04.008.
- [70] M. Fridrichová, K. Dvořák, D. Gazdič, J. Mokrá, K. Kulísek, Thermodynamic stability of ettringite formed by hydration of ye'elimite clinker, Ann. Mater. Sci. Eng. (2016), https://doi.org/10.1155/2016/9280131.